

See discussions, stats, and author profiles for this publication at: <https://www.researchgate.net/publication/11885184>

# 2-Deoxy-beta-D-erythro-pentofuranose: hydroxymethyl group conformation and substituent effects on molecular structure, ring geometry, and NMR spin-spin coupling constants from quan...

ARTICLE *in* JOURNAL OF THE AMERICAN CHEMICAL SOCIETY · JUNE 2001

Impact Factor: 12.11 · Source: PubMed

---

CITATIONS

8

---

READS

13

3 AUTHORS, INCLUDING:



Francis Cloran

Wright-Patterson Air Force Base

14 PUBLICATIONS 385 CITATIONS

SEE PROFILE

## 2-Deoxy- $\beta$ -D-erythro-pentofuranose: Hydroxymethyl Group Conformation and Substituent Effects on Molecular Structure, Ring Geometry, and NMR Spin–Spin Coupling Constants from Quantum Chemical Calculations

Francis Cloran,<sup>†</sup> Ian Carmichael,<sup>‡</sup> and Anthony S. Serianni<sup>\*,†</sup>

Contribution from the Department of Chemistry and Biochemistry, and the Radiation Laboratory, University of Notre Dame, Notre Dame, Indiana 46556

Received July 11, 2000. Revised Manuscript Received February 7, 2001

**Abstract:** The effect of hydroxymethyl conformation (*gg*, *gt*, and *tg* rotamers about the C4–C5 bond) on the conformational energies and structural parameters (bond lengths, bond angles, bond torsions) of the 10 envelope forms of the biologically relevant aldopentofuranose, 2-deoxy- $\beta$ -D-erythro-pentofuranose (2-deoxy-D-ribofuranose) **2**, has been investigated by ab initio molecular orbital calculations at the HF/6-31G\* level of theory. C4–C5 bond rotation induces significant changes in the conformational energy profile of **2** (*2gt* and *2tg* exhibit one global energy minimum, whereas *2gg* exhibits two nearly equivalent energy minima), and structural changes, especially those in bond lengths, are consistent with predictions based on previously reported vicinal, 1,3- and 1,4-oxygen lone pair effects. HF/6-31G\*-optimized envelope geometries of *2gg* were re-optimized using density functional theory (DFT, B3LYP/6-31G\*), and the resulting structures were used in DFT calculations of NMR spin–spin coupling constants involving <sup>13</sup>C (i.e.,  $J_{CH}$  and  $J_{CC}$  over one, two, and three bonds) in *2gg* according to methods described previously. The computed  $J$ -couplings were compared to those reported previously in *2gt* to assess the effect of C4–C5 bond rotation on scalar couplings within the furanose ring and hydroxymethyl side chain. The results confirm prior predictions of correlations between  $^2J_{CH}$ ,  $^3J_{CH}$ ,  $^2J_{CC}$  and  $^3J_{CC}$ , and ring conformation, and verify the usefulness of a concerted application of these couplings (both their magnitudes and signs) in assigning preferred ring and C4–C5 bond conformations in aldopentofuranosyl rings. The new calculated  $J$ -couplings in *2gg* have particular relevance to related  $J$ -couplings in DNA (and RNA indirectly), where the *gg* rotamer, rather than the *gt* rotamer, is observed in most native structures. The effects of two additional structural perturbations on **2** were also studied, namely, deoxygenation at C5 (yielding 2,5-dideoxy- $\beta$ -D-erythro-pentofuranose **4**) and methyl glycosidation at O1 (yielding methyl 2-deoxy- $\beta$ -D-erythro-pentofuranoside **5**) at the HF/6-31G\* level. The conformational energy profile of **4** resembles that found for *2gt*, not *2gg*, indicating that **4** is an inappropriate structural mimic of the furanose ring in DNA. Glycosidation failed to induce differential stabilization of ring conformations containing an axial C1–O1 bond (anomeric effect), contrary to experimental data. The latter discrepancy indicates that either the magnitude of this differential stabilization depends on ring configuration or that solvent effects, which are neglected in these calculations, play a role in promoting this stabilization.

### Introduction

The  $\beta$ -D-ribofuranose **1** and 2-deoxy- $\beta$ -D-erythro-pentofuranose **2** (2-deoxy- $\beta$ -D-ribofuranose) constituents of RNA and DNA play key roles in conferring conformational flexibility to these important biopolymers.<sup>1</sup> While considerable effort has been devoted to understanding their conformational properties using a range of experimental and theoretical methods,<sup>2</sup> experimental determinations are often limited by insufficient parameters on which to assign conformation or to test predictions of conformation and dynamics based on theoretical approaches. <sup>1</sup>H–<sup>1</sup>H  $J$ -couplings and NOEs are commonly used to assess solution properties of furanosyl rings,<sup>3</sup> but these parameters are

relatively few in number and are not without their limitations. This problem can, in principle, be reduced if additional structural constraints are obtained from scalar or dipolar couplings involving <sup>13</sup>C; for example, 17 *intra-ring*  $J_{CH}$  values exist in **1** compared to only 3  $^3J_{HH}$  values, but the former data are virtually ignored at present.<sup>4</sup> While the potential value of these parameters is self-evident, their use has been hampered by insufficient quantitative correlations between their magnitudes and molecular structure. Recent improvements in <sup>13</sup>C-labeling methodology<sup>5</sup> and in theoretical treatments of NMR  $J$ -couplings<sup>6</sup> now allow these correlations to be established. Thus, the suggestion<sup>7a</sup> that **1** and **2** assume a two-state conformational equilibrium in solution, characterized by exchange between generic N (north) (<sup>3</sup>E) and S (south) (<sup>2</sup>E) conformers predominantly via the eastern pathway of a pseudorotational itinerary (Scheme 1),<sup>3i,7b</sup> can be subjected to more rigorous experimental scrutiny. While this model has been widely accepted and invoked,<sup>7c,d</sup> it remains unclear whether it applies to all furanosyl rings regardless of

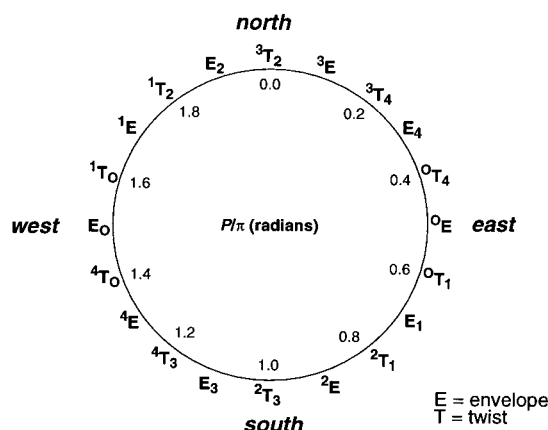
\* Author for correspondence.

<sup>†</sup> Department of Chemistry and Biochemistry.

<sup>‡</sup> Radiation Laboratory.

(1) (a) Westhof, E.; Sundaralingam, M. *J. Am. Chem. Soc.* **1983**, *105*, 970–976. (b) Westhof, E.; Sundaralingam, M. *J. Am. Chem. Soc.* **1980**, *102*, 1493–1500. (c) Levitt, M.; Warshel, A. *J. Am. Chem. Soc.* **1978**, *100*, 2607–2613.

Scheme 1



their configuration, state of substitution, or environment. Studies of furanosyl rings other than **1** and **2** have been rare, and systematic studies of ring-substitution effects are virtually nonexistent, although theoretical studies of methyl  $\alpha$ -arabino-furanoside appeared recently.<sup>8</sup>

Ab initio molecular orbital methods have been applied previously at various levels of theory to investigate the structural properties of **1** and **2** and to compute  $J$ -couplings ( $J_{CH}$ ,  $J_{CC}$ ) in these rings for comparison to those obtained by experiment.<sup>4,9</sup> In addition, the effect of replacing O1 of **2** with an amino group,

(2) (a) Olson, W. K. *J. Am. Chem. Soc.* **1982**, *104*, 278–286. (b) Olson, W. K.; Sussman, J. L. *J. Am. Chem. Soc.* **1982**, *104*, 270–278. (c) Harvey, S. C.; Prabhakaran, M. J. *Am. Chem. Soc.* **1986**, *108*, 6128–6136. (d) Pearlman, D. A.; Kim, S.-H. *J. Biomol. Struct. Dyn.* **1985**, *3*, 99–124. (e) Szyperki, T.; Fernandez, C.; Ono, A.; Kainosho, M.; Wüthrich, K. *J. Am. Chem. Soc.* **1998**, *120*, 821–822. (f) Schuerman, G. S.; Van Meervelt, L. *J. Am. Chem. Soc.* **2000**, *122*, 232–240. (g) Rinkel, L. J.; Altona, C. J. *Biomol. Struct. Dyn.* **1987**, *4*, 621–649. (h) Giessner-Pretre, C.; Pullman, B. *Q. Rev. Biophys.* **1987**, *20*, 113–172.

(3) (a) Van De Ven, F. J. M.; Hilbers, C. W. *Eur. J. Biochem.* **1988**, *178*, 1–38. (b) Chary, K. V. R.; Modi, S. *FEBS Lett.* **1988**, *233*, 319–325. (c) Radhakrishnan, I.; Patel, D. J.; Gao, X. *Biochemistry* **1992**, *31*, 2514–2523. (d) Kim, S.-G.; Lin, L.-J.; Reid, B. R. *Biochemistry* **1992**, *31*, 3564–3574. (e) Salazar, M.; Fedoroff, O. Y.; Miller, J. M.; Ribeiro, N. S.; Reid, B. R. *Biochemistry* **1993**, *32*, 4207–4215. (f) Majumdar, A.; Hosur, R. V. *Prog. Nucl. Magn. Reson. Spectrosc.* **1992**, *24*, 109–158. (g) Clore, G. M.; Gronenborn, A. M. *Crit. Rev. Biochem. Mol. Biol.* **1989**, *24*, 479–564. (h) Schwalbe, H.; Marion, J. P.; King, G. C.; Wechselberger, R.; Bermel, W.; Griesinger, C. *J. Biomol. NMR* **1994**, *4*, 631–644. (i) Altona, C.; Sundaralingam, M. *J. Am. Chem. Soc.* **1973**, *95*, 2333–2344.

(4) Podlasek, C. A.; Stripe, W. A.; Carmichael, I.; Shang, M.; Basu, B.; Serianni, A. S. *J. Am. Chem. Soc.* **1996**, *118*, 1413–1425.

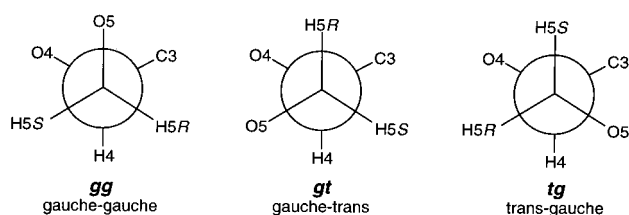
(5) (a) Lancelot, G.; Chanteloup, L.; Beau, J. M.; Thuong, N. T. *J. Am. Chem. Soc.* **1993**, *115*, 1599. (b) Sklenar, V.; Peterson, R. D.; Rejante, M. R.; Feigon, J. *J. Biomol. NMR* **1993**, *3*, 721. (c) Ono, A.; Tate, S.; Kainosho, M. *J. Biomol. NMR* **1994**, *4*, 581–586. (d) Wu, J.; Serianni, A. S. *Biopolymers* **1994**, *34*, 1175–1186. (e) Zimmer, D. P.; Crothers, D. M. *Proc. Natl. Acad. Sci. U.S.A.* **1995**, *92*, 3091–3095. (f) Nikonowicz, E. P.; Sirr, A.; Legault, P.; Jucker, F. M.; Baer, L. M.; Pardi, A. *Nucleic Acids Res.* **1992**, *20*, 4507–4513.

(6) (a) Carmichael, I. *J. Phys. Chem.* **1993**, *97*, 1789–92. (b) Bauschlicher, C. W., Jr.; Partridge, H. *Chem. Phys. Lett.* **1995**, *240*, 533–40. (c) Malkin, V. G.; Malkina, O. L.; Eriksson, L. A.; Salahub, D. R. In *The Calculation of NMR and ESR Spectroscopy Parameters Using Density Functional Theory*; Malkin, V. G., Malkina, O. L., Eriksson, L. A., Salahub, D. R., Eds.; Elsevier Science B.V.: New York, 1995; Vol. 2, pp 273–347. (d) Stahl, M.; Schopfer, U.; Frenking, G.; Hoffmann, R. W. *J. Org. Chem.* **1997**, *62*, 3702–3704. (e) Hricovini, M.; Malkina, O. L.; Bizik, F.; Nagy, L. T.; Malkin, V. G. *J. Phys. Chem. A* **1997**, *101*, 9756–9762.

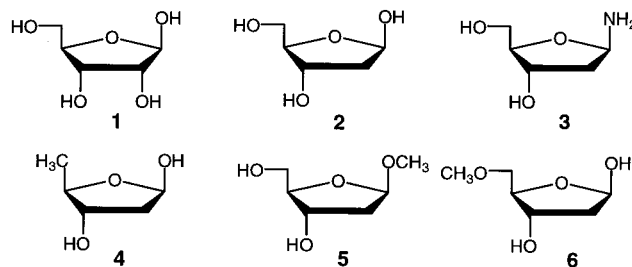
(7) (a) Raap, J.; van Boom, J. H.; van Lieshout, H. C.; Haasnoot, C. A. G. *J. Am. Chem. Soc.* **1988**, *110*, 2736–2743. (b) De Leeuw, H. P. M.; Haasnoot, C. A. G.; Altona, C. *Isr. J. Chem.* **1980**, *20*, 108–126. (c) Hoffmann, R. A.; van Wijk, J.; Leeftang, B. R.; Kamerling, J. P.; Altona, C.; Vliegthart, J. F. G. *J. Am. Chem. Soc.* **1992**, *114*, 3710. (d) Plavec, J.; Tong, W.; Chattopadhyaya, J. *J. Am. Chem. Soc.* **1993**, *115*, 9734–9746.

(8) Gordon, M. T.; Lowary, T. L.; Hadad, C. M. *J. Am. Chem. Soc.* **1999**, *121*, 9682–9692.

Scheme 2



yielding **3**, on computed conformational properties and  $J$ -couplings has been examined.<sup>10</sup> These investigations were restricted to a single rotamer about the C4–C5 bond, namely, that having O5 *anti* to C3 (*gt* rotamer, Scheme 2), to allow comparison of calculated  $J$ -couplings to those observed in solution, where the *gt* form predominates.<sup>11</sup> However, direct application of these prior findings to structural studies of nucleic acids is hampered, in part, by the fact that the *gg* rotamer is observed in these biopolymers.<sup>12</sup> Since our long-term objective is to apply these scalar couplings to DNA and RNA structure determinations, we were compelled to investigate the effect of C4–C5 bond rotation on conformational energies, structural properties, and NMR  $J$ -couplings ( $J_{CH}$  and  $J_{CC}$ ) in **2**. In addition, the effects of O5 deoxygenation and methyl glycosidation of **2**, giving **4** and **5**, respectively, on computed structures and conformational energies were studied. The latter studies were stimulated by the frequent use of 5-deoxy analogues in theoretical studies of **1** and **2**, leading to the question of how well these models mimic the real molecules. The present results yield new information on the effect of exocyclic conformation on structure and  $J$ -couplings in furanose rings of general importance to nucleic acid structure determination, new insights into factors that influence structure and geometry of aldofuranose rings, and the identification of important limitations in the use of structural mimics of **1** and **2**.



## Computational Methods

**A. Geometry Optimization.** Ab initio MO and DFT calculations were performed with a modified<sup>6a</sup> version of the Gaussian 94 suite of programs.<sup>13</sup> For geometric optimization at the Hartree–Fock (HF) and

(9) (a) Church, T. J.; Carmichael, I.; Serianni, A. S. *J. Am. Chem. Soc.* **1997**, *119*, 8946–8964. (b) Cloran, F.; Carmichael, I.; Serianni, A. S. *J. Phys. Chem.* **1999**, *103*, 3783–3795.

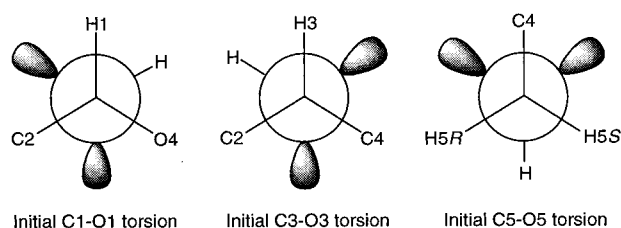
(10) Cloran, F.; Zhu, Y.; Osborn, J.; Carmichael, I.; Serianni, A. S. *J. Am. Chem. Soc.* **2000**, *122*, 6435–6448.

(11) Wu, G. D.; Serianni, A. S.; Barker, R. *J. Org. Chem.* **1983**, *48*, 1750–1757.

(12) Saenger, W. *Principles of Nucleic Acid Structure*; Springer-Verlag: New York, 1983.

(13) Frisch, M. J.; Trucks, G. W.; Schlegel, H. B.; Gill, P. M. W.; Johnson, B. G.; Robb, M. A.; Cheeseman, J. R.; Keith, T.; Petersson, G. A.; Montgomery, J. A.; Raghavachari, K.; Al-Laham, M. A.; Zakrzewski, V. G.; Ortiz, J. V.; Foresman, J. B.; Peng, C. Y.; Ayala, P. Y.; Chen, W.; Wong, M. W.; Andres, J. L.; Replogle, E. S.; Gomperts, R.; Martin, R. L.; Fox, D. J.; Binkley, J. S.; Defrees, D. J.; Baker, J.; Stewart, J. P.; Head-Gordon, M.; Gonzalez, C.; Pople, J. A. *Gaussian 94*; revision B.3 Gaussian, Inc.: Pittsburgh, PA, 1995.

## Scheme 3



DFT levels of theory, the polarized split-valence 6-31G\* basis set<sup>14</sup> was employed. For DFT, the standard B3LYP functional, due to Becke,<sup>15</sup> was used in all calculations. This functional comprises both local<sup>16</sup> and nonlocal<sup>17</sup> exchange contributions and contains terms accounting for local<sup>18</sup> and nonlocal<sup>19</sup> correlation corrections.

The 10 envelope forms of **2**, **4**, and **5** were examined by holding one endocyclic torsion angle fixed in each of 10 computations (i.e., for <sup>3</sup>E, the C4–O4–C1–C2 torsion was held constant at 0°), as described in prior work.<sup>4,9,10</sup> All remaining structural parameters were allowed to relax in each calculation unless otherwise noted. Individual envelope forms are identified throughout the manuscript by their corresponding pseudorotational phase angles,<sup>31</sup>  $P$  (Scheme 1), and are represented in graphical plots as  $P/\pi$  radians, where <sup>3</sup>E = 0.1  $P/\pi$  ( $P = 18^\circ$ ),  $E_4 = 0.3 P/\pi$  ( $P = 54^\circ$ ), and so forth.

**B. Calculations of NMR Spin–Spin Coupling Constants.** <sup>13</sup>C–<sup>1</sup>H and <sup>13</sup>C–<sup>13</sup>C NMR spin–spin coupling constants in the DFT-optimized structures were obtained by finite-field (Fermi-contact) double perturbation theory<sup>20</sup> calculations at the B3LYP level using a basis set ([5s2p1d,2s]) previously constructed for similar systems.<sup>6a</sup> Appropriate values for the perturbing fields imposed on the coupled nuclei were chosen to ensure sufficient numerical precision while still allowing a satisfactory low-order finite-difference representation of the effect of the perturbation. Only the Fermi contact component of each coupling constant was considered due to the dominant relationship of this term in  $J$  values involving carbon and hydrogen in saturated systems.

## Results and Discussion

**A. General Considerations.** All calculations on **2** were conducted as a function of pseudorotation phase angle  $P$  by holding one endocyclic torsion angle constant at 0° (see Computational Methods); this torsion was the only structural parameter held constant in the calculations unless otherwise noted. All 10 envelope forms were considered, and in each calculation the following *initial* exocyclic torsion angles were used: H1–C1–O1–H, 60°; H3–C3–O3–H, –60°; C4–C5–O5–H, 180° (Scheme 3). The C3–O3 and C5–O5 torsions were chosen arbitrarily, whereas the C1–O1 torsion was chosen to optimize the exoanomeric effect.<sup>21</sup> Initial C4–C5 torsion angles were chosen to orient the hydroxymethyl side chain in the *gg*, *gt* and *tg* conformations (Scheme 2). A total of 30 structures of **2** were examined, that is, 10 envelope forms of **2** in each of the three hydroxymethyl group conformations (hereafter denoted **2gg**, **2gt** and **2tg**).

Calculations on **5** were conducted in the *gt* conformation only, and initial exocyclic torsion angles (C1–O1, C3–O3, C5–O5) were the same as used for **2**. Calculations on **4** also used the

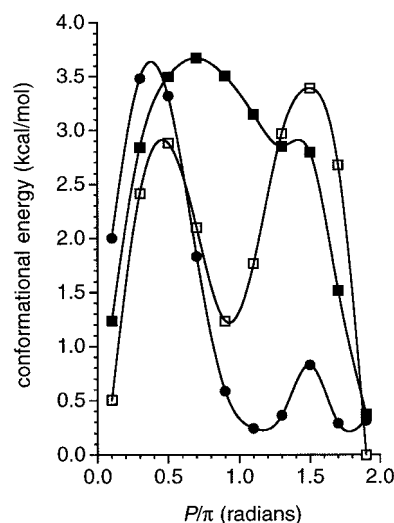


**Figure 1.** Conformational energy profiles for **2** as a function of hydroxymethyl group rotation (HF/6-31G\*). Closed squares, *gt*; open squares, *gg*; closed circles, *tg* (Scheme 2). One full rotation around the pseudorotational itinerary is equivalent to 0–2  $P/\pi$ , where 0.1  $P/\pi = ^3E$ , 0.3  $P/\pi = E_4$ , 0.5  $P/\pi = ^1E$ , and so forth (Scheme 1).

same initial C1–O1 and C3–O3 exocyclic torsion angles applied to **2**. Ten envelope geometries of **4** and **5** were examined.

Geometric optimizations proceeded smoothly for the 10 envelope forms of **2gt**; changes in the initial exocyclic bond torsions were minimal, yielding optimized structures conformationally similar to the initial geometries. However, four **2gg** conformers ( $E_3$ , <sup>4</sup>E, <sup>1</sup>E, and  $E_2$ ) and three **2tg** conformers ( $E_2$ , <sup>3</sup>E, and  $E_4$ ) experienced significant exocyclic bond rotations during geometric optimization. In  $E_3$  and <sup>4</sup>E of **2gg**, the C4–C5–O5–H torsion changed from  $\sim 180^\circ$  to  $\sim 60^\circ$  upon optimization, which was presumably driven by the formation of an intramolecular hydrogen bond between O1 and O5–H. In <sup>1</sup>E and  $E_2$  of **2gg**, the H1–C1–O1–H torsion angle changed from  $\sim 60^\circ$  to  $\sim 150^\circ$ ; again intramolecular hydrogen bonding between O5 and O1–H appeared responsible. In  $E_2$ , <sup>3</sup>E, and  $E_4$  of **2tg**, the C2–C3–O3–H torsion angle changed from  $\sim 60^\circ$  to  $\sim 180^\circ$ , presumably driven by hydrogen bonding between O5 and O3–H. The occurrence of these spontaneous transitions during geometric optimization complicated the calculations, since the resulting structures could not be reliably compared energetically or structurally. To avoid this problem, the relevant torsion angles were held constant during geometric optimization of these structures, with the realization that the additional structural constraints introduce uncertainty in the subsequent analysis of conformational energies, structural parameters, and  $J$ -couplings. We reasoned, however, that errors introduced as a result of employing a second geometric constraint would be less serious than those introduced by comparing significantly different structures; this is especially true for conformational energies, since the presence of a hydrogen bond in some structures but not in others would lead to an erroneous assessment of preferred conformation. We sought to keep the number and type of interactions as constant as possible between conformers to permit a more reliable comparison of energy and structure. In the following discussion, these additional constraints are identified when there is reason to believe that they may influence the interpretation of results.

**B. Effect of Hydroxymethyl Group Conformation on the Conformational Energy and Structure of 2.** The conformational energy profiles of **2gg**, **2gt**, and **2tg** (Figure 1) differ

(14) Hehre, W. J.; Ditchfield, R.; Pople, J. A. *J. Chem. Phys.* **1972**, *56*, 2257–2261.

(15) Becke, A. D. *J. Chem. Phys.* **1993**, *98*, 5648–5652.

(16) Slater, J. C. *The Self-Consistent Field for Molecules and Solids*; McGraw-Hill: New York, 1974.

(17) Becke, A. D. *ACS Symp. Ser.* **1989**, *394*, 165.

(18) Vosko, S. H.; Wilk, L.; Nusair, M. *Can. J. Phys.* **1980**, *58*, 1200.

(19) Lee, C.; Yang, W.; Parr, R. G. *Phys. Rev. B* **1988**, *37*, 785.

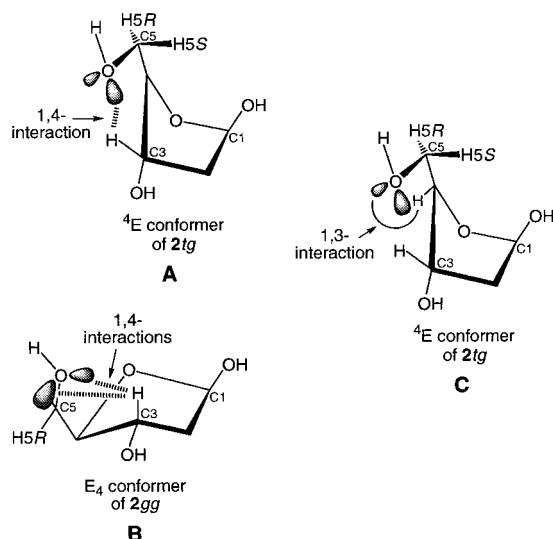
(20) Kowalewski, J.; Laaksonen, A.; Roos, B.; Siegbahn, P. *J. Chem. Phys.* **1979**, *71*, 2896–2902.

(21) (a) Lemieux, R. U.; Koto, S. *Tetrahedron* **1974**, *30*, 1933–1944.

(b) Praly, J.-P.; Lemieux, R. U. *Can. J. Chem.* **1987**, *65*, 213–223. (c) Lemieux, R. U. *Pure Appl. Chem.* **1971**, *25*, 527–548.



Scheme 4



significantly. The *global* minimum energy structure is **2gg** in the  $E_2$  conformation; the same conformation lies at the energy minimum for **2gt** but not **2tg** ( $E_3$ ). A comparison of the energy profiles for **2gt** and **2tg** shows that southern and western conformations of the latter are stabilized relative to the same conformations in the former. Interestingly, the conformational energy profile for **2gg** is biphasic, showing defined energy minima in the N and S regions of the itinerary, whereas that for **2gt** shows a single minimum and for **2tg** an extended, relatively flat region from 1 to 2.0  $P/\pi$ . The conformational behavior exhibited by **2gg** is consistent with the widely applied two-state N/S conformational model, in contrast to those of **2gt** and **2tg**. These data show that hydroxymethyl conformation influences the conformational energy profile of **2** significantly.

Activation barriers to pseudorotation for **2gg**, **2gt**, and **2tg** are similar. Conformational energies determined for the planar geometries of **2gg** and **2gt** are  $\sim 0.3$  and  $\sim 1.4$  kcal/mol, respectively, *higher* in energy than the least stable envelope form, whereas the planar **2tg** form is  $\sim 0.4$  kcal/mol *lower* in energy than the least stable envelope form. Thus, nonplanar conformer interconversion via pseudorotation for **2gg** and **2gt** appears more favored than that via an inversion pathway, but inversion may play a role in nonplanar conformer exchange for **2tg**.

The dependencies of the C1–H1 and C2–H2R bond lengths on ring conformation are not affected significantly by hydroxymethyl conformation, whereas the behaviors of the C2–H2S, C3–H3, and C4–H4 bond lengths differ (see Supporting Information, Figure 1). The conformational dependence of the C3–H3 bond differs in each C4–C5 rotamer, with the longest bonds predicted in **2gt**. Presumably bond shortening in **2gg** and **2tg** is caused by 1,4-lone pair effects involving O5,<sup>10</sup> which are stronger in ring conformations between 0.5 and 1.5  $P/\pi$  (south (S) forms, Scheme 1) for **2tg** (Scheme 4, A). The further reduction in length found in ring conformations between 1.5 and 0.5  $P/\pi$  (north (N) forms, Scheme 1) for **2gg** relative to **2tg** may be caused by the additive effects of the O5 lone-pairs, *both* of which are in proximity to H3 in these conformations (Scheme 4, B); in S forms, only one O5 lone-pair is near H3, and thus the effect mimics that found in S forms of **2tg**. The behavior of the C4–H4 bond length is similar for **2gg**, **2gt**, and **2tg**, but the curves for **2gt** and **2tg** are displaced to slightly shorter bond lengths. This shortening is caused by the presence

of 1,3-lone-pair effects<sup>22</sup> from O5 on the C4–H4 bond in **2gt** and **2tg** (Scheme 4, C); this effect is absent in **2gg**.

Corresponding C–C bond lengths exhibit similar dependencies on ring conformation in **2gg**, **2gt**, and **2tg** (see Supporting Information, Figure 2). The exocyclic C1–O1 bond length in **2gg** is consistently shorter in west conformers (see Supporting Information, Figure 3). This bond is expected to lengthen when quasi-axial (i.e., in  $^1E$ ),<sup>9b,23–25</sup> due to bond orientation and to  $n_{O4} \rightarrow \sigma_{C1,O1}^*$  lone-pair donation (also causes C1–O4 bond contraction; see below). The suppressed bond lengthening in **2gg** may partly explain the higher-energy western forms of **2gg** relative to those for **2gt** and **2tg** (Figure 1), an argument supported by the behavior of the C1–O4 bond in **2gg** discussed below. The exocyclic C3–O3 bond length shows the same general dependence on ring conformation, but appears uniformly longer in **2gg** (see Supporting Information, Figure 3).

The endocyclic C1–O4 bond length decreases in length significantly in western conformers of **2gt** and **2tg** relative to those of **2gg** (see Supporting Information, Figure 3), suggesting less potent O4 lone-pair donation in **2gg** and possibly explaining the higher energy of western conformers of **2gg** relative to those of **2gt** and **2tg**. The C4–O4 (and C4–C5; see above) bond lengths are longer for **2tg** relative to those for **2gg** and **2gt** (see Supporting Information, Figure 3). In contrast, the exocyclic C5–O5 bond length exhibits a significantly different dependence on ring conformation in **2gg**, **2gt**, and **2tg** (see Supporting Information, Figure 3), which is attributed to the influence of O3 and O4 lone-pair effects on this bond.

Puckering amplitude ( $\tau_m$ ) is smaller in west forms of **2gg** relative to those of **2gt** and **2tg** (see Supporting Information, Figure 4), presumably caused by minimization of destabilizing 1,3 interactions between O1 and C5. A relatively large decrease in  $\tau_m$  is also observed in  $E_4$  of **2tg**, presumably caused by the avoidance of 1,3-interactions between O3 and O5.

Changes in the exocyclic C1–O1, C3–O3, C5–O5, and C4–C5 torsion angles with ring conformation for **2gg**, **2gt**, and **2tg** are small (data not shown), with discontinuities caused by the need to “fix” these torsions in some ring conformations (see above).

**C. Comparison of NMR Spin–Spin Coupling Constants ( $J_{CH}$  and  $J_{CC}$ ) in **2gg** and **2gt**.** The 10 envelope forms of **2gg** which were geometrically optimized at the HF/6-31G\* level of theory were re-optimized using density functional theory (DFT, B3LYP/6-31G\*), and the resulting structures used to calculate  $J_{CH}$  and  $J_{CC}$  values from DFT as described previously.<sup>9b,26,27</sup> In the following discussion, these couplings are compared to corresponding values in **2gt**, which were computed previously using identical calculational methods.<sup>9b</sup>

**1.  $^1J_{CH}$ .** The conversion of **2gt** to **2gg** is accompanied by substantial changes in C–H bond lengths on the same face of the ring (i.e., C2–H2S and C3–H3) and smaller but discernible changes in C–H bonds on the opposite face (i.e., C1–H1, C2–H2R, C4–H4). Given that C–H bond length is an important determinant of  $^1J_{CH}$  magnitude, substantial differences in  $^1J_{C2,H2S}$

(22) Kennedy, J.; Wu, J.; Drew, K.; Carmichael, I.; Serianni, A. S. *J. Am. Chem. Soc.* **1997**, *119*, 8933–8945.

(23) Juaristi, E.; Cuevas, G. *The Anomeric Effect*; CRC Press: Boca Raton, FL, 1995.

(24) Lemieux, R. U. In *Molecular Rearrangements*; de Mayo, P., Ed.; Wiley-Interscience: New York, 1963; p 713.

(25) Cossé-Barbi, A.; Dubois, J.-E. *J. Am. Chem. Soc.* **1987**, *109*, 1503–1511.

(26) Cloran, F.; Carmichael, I.; Serianni, A. S. *J. Am. Chem. Soc.* **1999**, *121*, 9843–9851.

(27) Cloran, F.; Carmichael, I.; Serianni, A. S. *J. Am. Chem. Soc.* **2000**, *122*, 396–397.

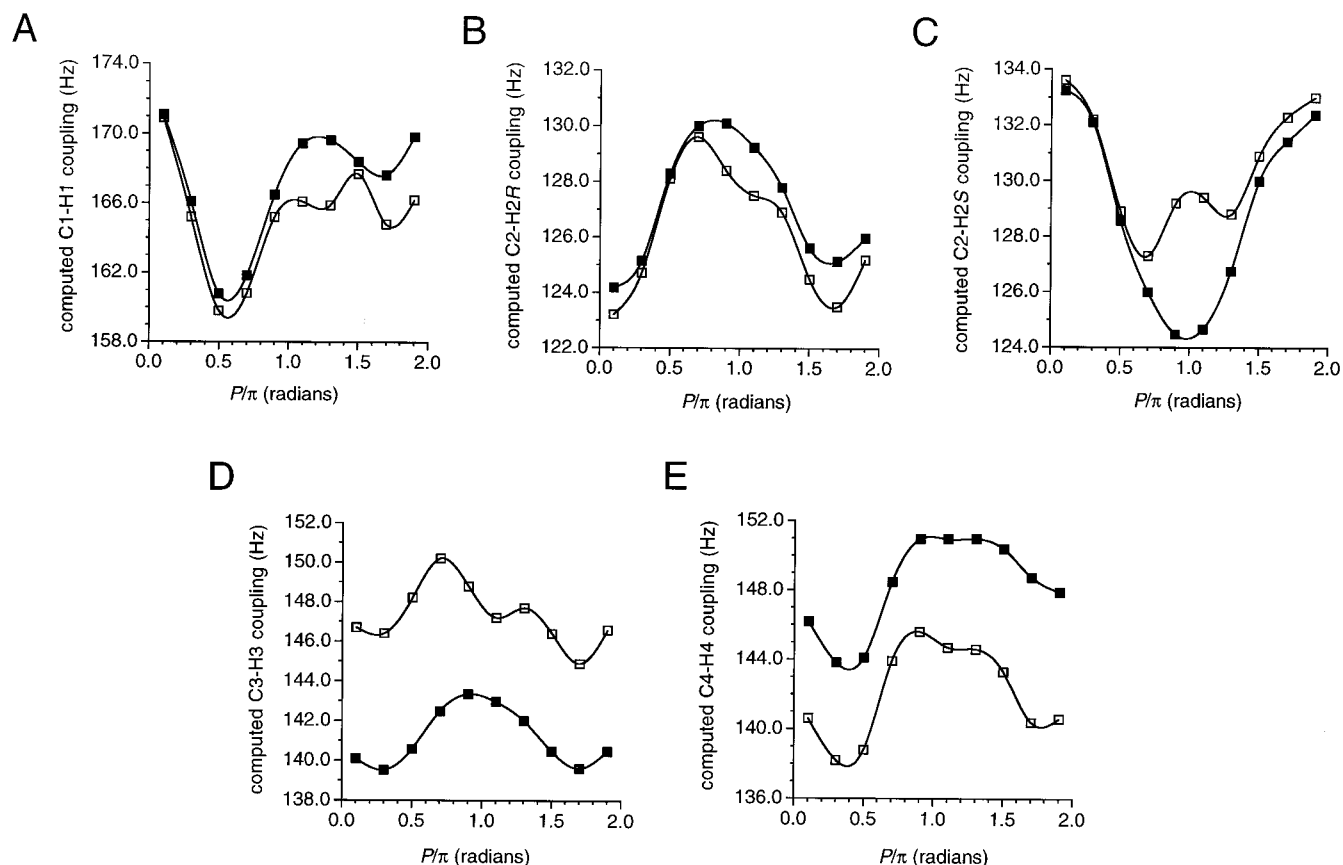


**Figure 2.** Computed intra-ring  $^1J_{CH}$  values in  $2gt$  (solid squares) and  $2gg$  (open squares) determined from density functional theory (optimized geometries: B3LYP/6-31G\*;  $J$ -coupling calculations: B3LYP/[5s2p1d,2s]). (A)  $^1J_{C1,H1}$ . (B)  $^1J_{C2,H2R}$ . (C)  $^1J_{C2,H2S}$ . (D)  $^1J_{C3,H3}$ . (E)  $^1J_{C4,H4}$ .

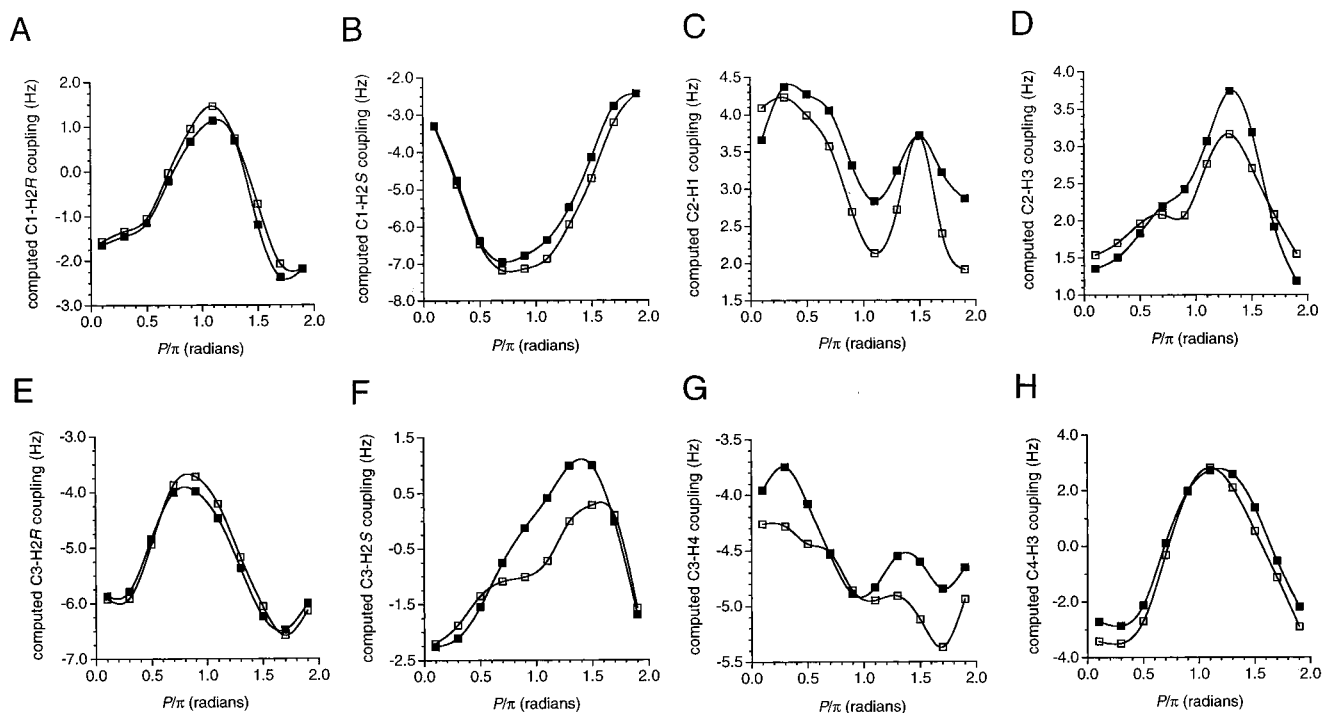


**Figure 3.** Computed intra-ring  $^2J_{CH}$  values in  $2gt$  (solid squares) and  $2gg$  (open squares) determined from density functional theory (optimized geometries: B3LYP/6-31G\*;  $J$ -coupling calculations: B3LYP/[5s2p1d,2s]). (A)  $^2J_{C1,H2R}$ . (B)  $^2J_{C1,H2S}$ . (C)  $^2J_{C2,H1}$ . (D)  $^2J_{C2,H3}$ . (E)  $^2J_{C3,H2R}$ . (F)  $^2J_{C3,H3}$ . (G)  $^2J_{C3,H4}$ . (H)  $^2J_{C4,H3}$ .

and  $^1J_{C3,H3}$  are expected between  $2gt$  and  $2gg$ . For C2–H2S, substantial local differences are observed in S conformers, where larger  $^1J_{C2,H2S}$  are observed in  $2gg$  (Figure 2C); the larger couplings correlate with the shorter C2–H2S bonds found in

these conformers of  $2gg$ . In contrast,  $^1J_{C3,H3}$  is uniformly larger in  $2gg$  than in  $2gt$  (Figure 2D), consistent with the uniformly shorter bonds in the former. The C4–H4 bond lengths are also uniformly longer in  $2gg$  than in  $2gt$ , translating into uniformly

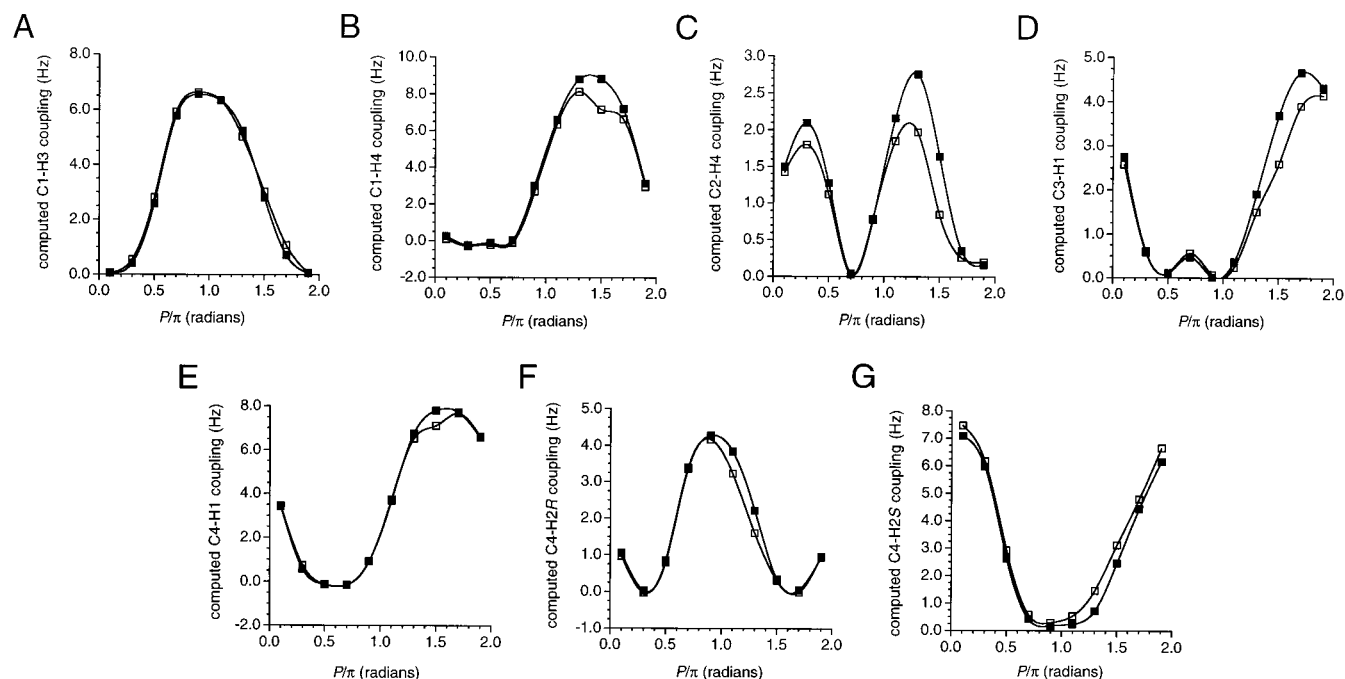


**Figure 4.** Computed intra-ring  $^3J_{CH}$  values in **2gt** (solid squares) and **2gg** (open squares) determined from density functional theory (optimized geometries: B3LYP/6-31G\*;  $J$ -coupling calculations: B3LYP/[5s2p1d,2s]). (A)  $^3J_{C1,H3}$ . (B)  $^3J_{C1,H4}$ . (C)  $^3J_{C2,H4}$ . (D)  $^3J_{C3,H1}$ . (E)  $^3J_{C4,H1}$ . (F)  $^3J_{C4,H2R}$ . (G)  $^3J_{C4,H2S}$ .

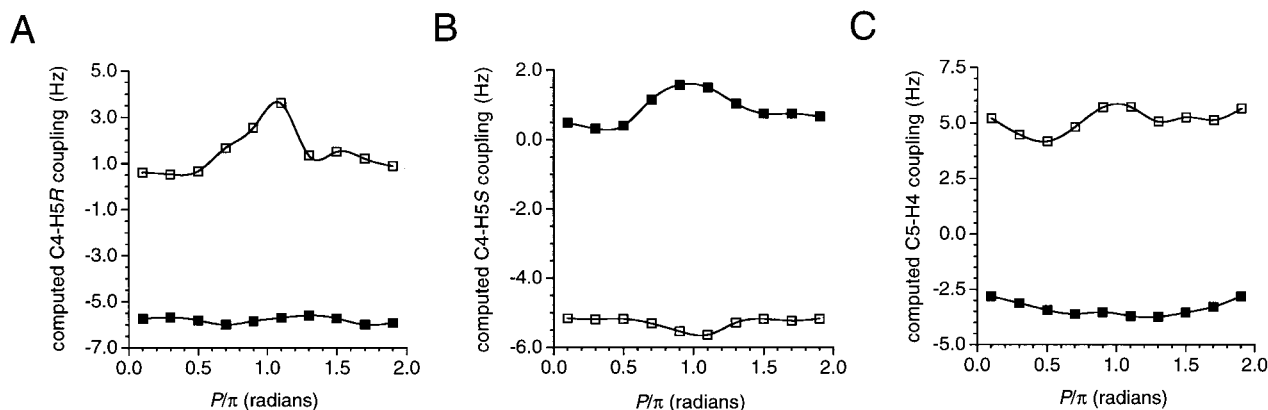


**Figure 5.** Computed hydroxymethyl  $^2J_{CH}$  values in **2gt** (solid squares) and **2gg** (open squares) determined from density functional theory (optimized geometries: B3LYP/6-31G\*;  $J$ -coupling calculations: B3LYP/[5s2p1d,2s]). (A)  $^2J_{C4,H5R}$ . (B)  $^2J_{C4,H5S}$ . (C)  $^2J_{C5,H4}$ .

smaller  $^1J_{C4,H4}$  in the former (Figure 2E). Local, smaller differences are observed for  $^1J_{C1,H1}$  and  $^1J_{C2,H2R}$  (Figure 2A,B) and also correlate with differences in C–H bond length, with shorter bonds yielding larger couplings. These results show that structural factors that influence C–H bond length, such as the orientation of large substituents (e.g.,  $-\text{CH}_2\text{OH}$ ) “over” the furanose ring, can cause significant changes in  $^1J_{CH}$  magnitude.

**2.  $^2J_{CH}$  (Intra-ring).** The dependencies of  $^2J_{C1,H2R}$ ,  $^2J_{C1,H2S}$ ,  $^2J_{C3,H2R}$ , and  $^2J_{C4,H3}$  on ring conformation are virtually identical in **2gt** and **2gg** (Figure 3). While larger differences appear to exist for  $^2J_{C2,H1}$ ,  $^2J_{C2,H3}$ , and  $^2J_{C3,H4}$ , these differences ( $< \sim 0.5$  Hz) are comparable to those observed in the above intra-ring  $^2J_{CH}$  (note the different scales on the y-axes of plots in Figure 3).  $^2J_{C3,H2S}$  exhibits the largest difference (Figure 3F), being smaller in **2gg** in S and W conformers (difference of  $\sim -1$  Hz). In general, the intra-ring  $^2J_{CH}$  values are not affected significantly by the conversion of **2gt** to **2gg**, with  $^2J_{C3,H2S}$  being a possible exception.

**3.  $^3J_{CH}$  (Intra-ring).** The dependencies of intra-ring  $^3J_{CH}$  on ring conformation are virtually identical in **2gt** and **2gg** (Figure 4). Small, local differences are attributed to the geometric

constraints imposed on several **2gg** conformers (see above) or to differences in C–H torsion angles (e.g., the significantly reduced puckering amplitude in W forms of **2gg** translates into smaller C–H torsion angles and thus into smaller  $^3J_{CH}$ ). The aberrant behavior of  $^3J_{C2,H4}$  reported previously in **2gt**<sup>9a,b</sup> is also observed in **2gg** (Figure 4C), reinforcing the contention that this coupling is less useful than the remaining  $^3J_{CH}$  as a conformational probe.

**4.  $^2J_{CH}$  and  $^3J_{CH}$  (Hydroxymethyl).** Six  $J_{CH}$  values involve coupled atoms in the hydroxymethyl group of **2**, and their magnitudes/signs are affected by hydroxymethyl conformation. These couplings include three  $^2J_{CH}$  ( $^2J_{C4,H5R}$ ,  $^2J_{C4,H5S}$ ,  $^2J_{C5,H4}$ ; Figure 5) and three  $^3J_{CH}$  ( $^3J_{C3,H5R}$ ,  $^3J_{C3,H5S}$ ,  $^3J_{C5,H3}$ ; Figure 6).

$^2J_{C4,H5R}$  and  $^2J_{C5,H4}$  are substantially more positive in **2gg** than in **2gt** ( $^2J_{C4,H5R}$  is  $\sim -6$  Hz in **2gt** and  $\sim 2$  Hz in **2gg**;  $^2J_{C5,H4}$  is  $\sim -3$  Hz in **2gt** and  $\sim 5$  Hz in **2gg**) (Figure 5A,C). In contrast,  $^2J_{C4,H5S}$  is substantially more negative in **2gg** ( $\sim -5$  Hz) than in **2gt** ( $\sim 1$  Hz) (Figure 5B). Recent experimental and theoretical studies have yielded correlations between hydroxymethyl conformation and the magnitudes/signs of these geminal  $^{13}\text{C}$ –

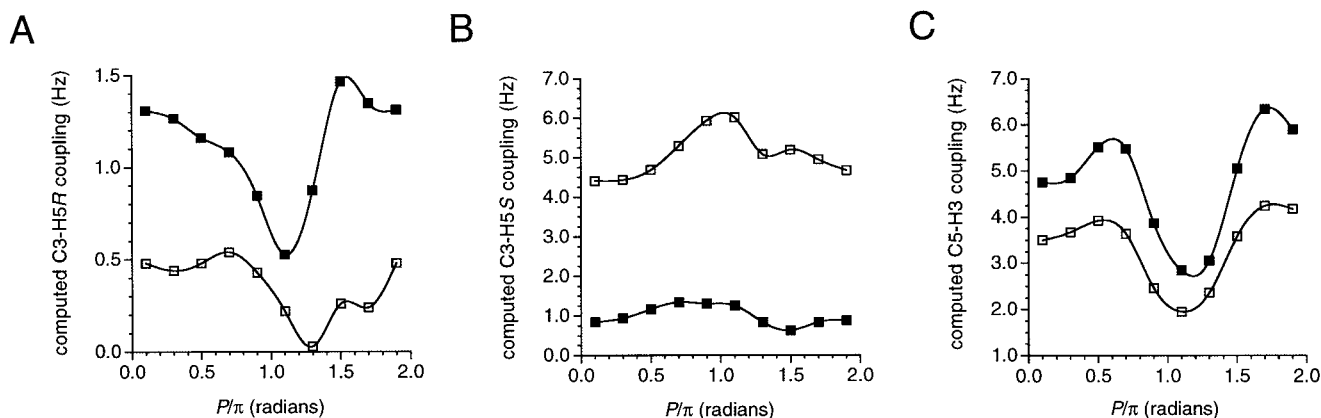


**Figure 6.** Computed hydroxymethyl  $^3J_{CH}$  values in **2gt** (solid squares) and **2gg** (open squares) determined from density functional theory (optimized geometries: B3LYP/6-31G\*;  $J$ -coupling calculations: B3LYP/[5s2p1d,2s]). (A)  $^3J_{C3,H5R}$ . (B)  $^3J_{C3,H5S}$ . (C)  $^3J_{C5,H3}$ .

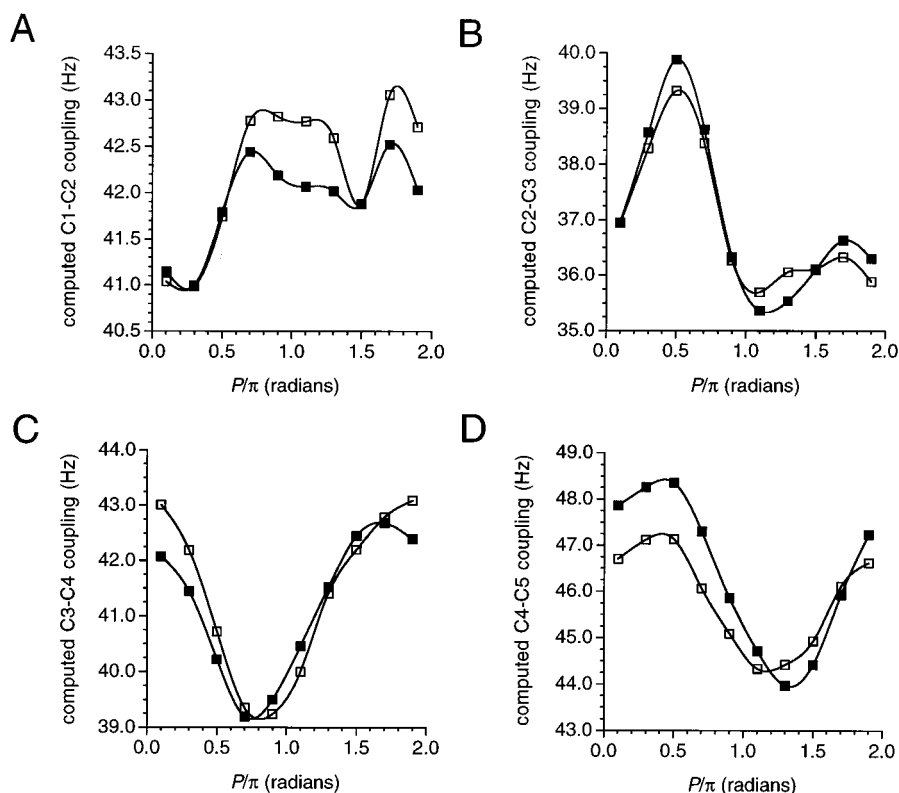


**Figure 7.** Computed  $^1J_{CC}$  values in **2gt** (solid squares) and **2gg** (open squares) determined from density functional theory (optimized geometries: B3LYP/6-31G\*;  $J$ -coupling calculations: B3LYP/[5s2p1d,2s]). (A)  $^1J_{C1,C2}$ . (B)  $^1J_{C2,C3}$ . (C)  $^1J_{C3,C4}$ . (D)  $^1J_{C4,H5}$ .

$^1H$  couplings,<sup>9a,28,29</sup> and the present results provide a means to test these predictions. Using an empirical projection sum,<sup>30</sup>  $^2J_{C4,H5R}$  was predicted to be (+) large in **2gg** and (−) small in **2gt**,  $^2J_{C4,H5S}$  was predicted to be (−) small in **2gg** and (+) large in **2gt**, and  $^2J_{C5,H4}$  was predicted to be (+) large in **2gg** and (−) small in **2gt** (see Table 5 in ref 9a). These predicted trends are consistent with the present data with regard to coupling sign, but inconsistent with respect to coupling magnitude. The latter inconsistency was documented recently;<sup>9b</sup> in general, the positive and negative  $^2J_{CH}$  have smaller and larger magnitudes, respectively, than predicted by the empirical projection sum, especially for  $^2J_{C4,H5R}$  and  $^2J_{C5,H5S}$ . Importantly, these new results confirm

the value of  $^2J_{CH}$  as general experimental probes of hydroxymethyl conformation in saccharides, since both magnitude and sign vary substantially with bond conformation.

Correlations between  $^3J_{CH}$  and hydroxymethyl conformation are based on the known Karplus dependency of these vicinal couplings.<sup>31</sup> Thus,  $^3J_{C3,H5R}$  values are small in **2gt** and **2gg** since C3 and H5R are gauche in both conformers (Figure 6A). However, the couplings are not equivalent; smaller values are expected<sup>32a</sup> and are found in **2gg** where H5R is *anti* to O4.  $^3J_{C3,H5S}$  is small in **2gt** (C3 and H5S gauche) and large in **2gg** (C3 and H5S *anti*) (Figure 6B). The cisoidal  $^3J_{C5,H3}$  shows the

(28) Hines, J. V.; Varani, G.; Landry, S. M.; Tinoco, I., Jr. *J. Am. Chem. Soc.* **1993**, *115*, 11002–11003.

(29) Marino, J. P.; Schwalbe, H.; Glaser, S. J.; Griesinger, C. *J. Am. Chem. Soc.* **1996**, *118*, 4388–4395.

(30) Bock, K.; Pedersen, C. *Acta Chem. Scand. Ser. B* **1977**, *31*, 354–358.

(31) (a) Schwarcz, J. A.; Perlin, A. S. *Can. J. Chem.* **1972**, *50*, 3667–3676. (b) Spoormaker, T.; de Bie, M. J. A. *Recl. Trav. Chim. Pays-Bas* **1978**, *97*, 85–87. (c) Tvaroska, I.; Gajdos, J. *Carbohydr. Res.* **1995**, *271*, 151–162.

(32) (a) Günther, H. *NMR Spectroscopy*; John Wiley and Sons: New York, 1995; p 119. (b) Marshall, J. L.; Walter, S. R.; Barfield, M.; Marchand, A. P.; Marchand, N. W.; Segre, A. L. *Tetrahedron* **1976**, *32*, 537–542.



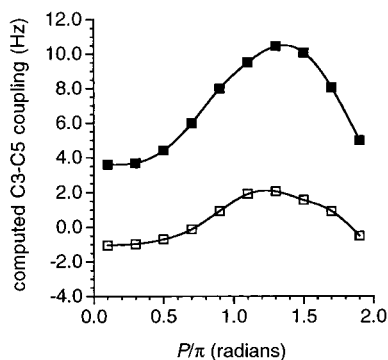


**Figure 8.** Computed  $^2J_{C3,C5}$  values in **2gt** (solid squares) and **2gg** (open squares) determined from density functional theory (optimized geometries: B3LYP/6-31G\*;  $J$ -coupling calculations: B3LYP/[5s2p1d,2s]).

expected biphasic dependency but with dissimilar maxima and minima (Figure 6C). For example,  $^3J_{C5,H3}$  in  $E_1$  is smaller than  $^3J_{C5,H3}$  in  $^1E$  in both **2gt** and **2gg**, and differences in the C5–C4–C3–H3 torsion angles in  $E_1$  and  $^1E$  do not fully explain the predicted trend. This behavior may be caused by a Barfield effect<sup>32b,33</sup> on cisoidal  $^3J_{CH}$  in furanose rings, although further study is needed to confirm this explanation.

**5.  $^1J_{CC}$ .** Overall coupling trends are conserved for endo- and exocyclic  $^1J_{CC}$  in **2gt** and **2gg** (Figure 7A–C). The exocyclic  $^1J_{C4,C5}$  exhibits the expected dependency on ring conformation in both **2gt** and **2gg** (Figure 7D), being largest when the C4–C5 bond is quasi-equatorial ( $E_4$ ) and smallest when this bond is quasi-axial ( $^4E$ ). Differences between **2gg** and **2gt** may be caused by the reported dependence of  $^1J_{CC}$  on O–C–C–O torsion angles.<sup>34</sup>

**6.  $^2J_{CC}$ .** One geminal  $J_{CC}$  exists in **2gt** and **2gg**, namely,  $^3J_{C3,C5}$ , and a relationship between  $^2J_{C3,C5}$  magnitude/sign and hydroxymethyl conformation has been predicted recently<sup>9b</sup> on the basis of an empirically derived projection resultant method.<sup>35</sup> As shown in Figure 8,  $^2J_{C3,C5}$  is (+) large in **2gt** but (±) small in **2gg**, in excellent agreement with the prior predictions. The smaller coupling magnitudes in **2gg** are caused by the inability of O5 to attain an in-plane geometry with the O3–C3–C4–C5 fragment, a geometry achievable in  $^4E$  of **2gt** where  $^2J_{C3,C5}$  is maximal. While the sensitivity of  $^2J_{C3,C5}$  to ring conformation in **2gg** is reduced relative to **2gt**, in agreement with prior predictions,<sup>9b</sup> the combined magnitude and sign change may still be sufficient to warrant the use of  $^2J_{C3,C5}$  as a conformational constraint in structural studies of nucleic acids containing the *gg* rotamer.

**7.  $^3J_{CC}$ .** Correlations between  $^3J_{C1,C5}$  and ring conformation in **2gt** and **2gg** are virtually identical (Figure 9A) and follow the Karplus dependency reported for C–O–C–C coupling fragments.<sup>26,36</sup> In addition to torsion angle,  $^3J_{COCC}$  values are influenced by the orientation of terminal electronegative substituents.<sup>26,36</sup> In **2gt** and **2gg**, one of the terminal electronegative substituents (O5) cannot achieve an in-plane orientation with respect to the O1–C1–O4–C5 fragment, thus explaining the similar curves (the C1–O4–C4–C5 torsion angle differences in **2gt** and **2gg** are relatively small). In contrast, the dependence of  $^3J_{C2,C5}$  on ring conformation is affected significantly by C4–C5 conformation (Figure 9B). The latter finding is explained

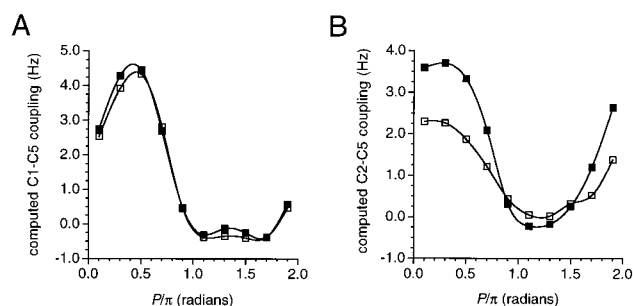


**Figure 9.** Computed  $^3J_{CC}$  values in **2gt** (solid squares) and **2gg** (open squares) determined from density functional theory (optimized geometries: B3LYP/6-31G\*;  $J$ -coupling calculations: B3LYP/[5s2p1d,2s]). (A)  $^3J_{C1,C5}$ . (B)  $^3J_{C2,C5}$ .

by noting that, in **2gt**, O5 can assume an in-plane orientation with respect to the C2–C3–C4–C5 fragment (in  $E_4$ ), whereas in **2gg**, this arrangement is not possible in any ring conformation. This difference translates into smaller couplings in **2gg** at geometries near  $E_4$ , relative to that in **2gt**, and confirms prior predictions.<sup>9b</sup>

**8.  $^{2+3}J_{CC}$ .** Three dual-pathway  $^{13}C$ – $^{13}C$  spin-couplings exist in **2**, namely,  $^{2+3}J_{C1,C3}$ ,  $^{2+3}J_{C1,C4}$ , and  $^{2+3}J_{C2,C4}$ . Overall correlations between these couplings and ring conformation are similar for **2gt** and **2gg** (Figure 10). Conversion of **2gt** to **2gg** leaves  $^{2+3}J_{C1,C4}$  essentially unaffected, whereas local changes (<1 Hz) are observed for the remaining two couplings. The most significant differences occur for  $^{2+3}J_{C2,C4}$  in *S* forms, where coupling is reduced in **2gg**. These results suggest that rotation of the C4–C5 bond exerts some effect on coupling along one or both of the contributing pathways, but the overall effect is relatively small.

**D. Substituent Effects on the Structure and Conformational Energy of 2. 1. C5-Deoxygenation.** Molecular orbital calculations (HF/6-31G\*) on **4** were performed to evaluate the effect of O5 deoxygenation on the structure and conformational energy of **2**. Since previous computational studies have used **4** as a structural model of the 2-deoxyribofuranose ring of DNA,<sup>2a,37</sup> we sought to determine whether this simplification is justified.

The conformational energy profile for **4** is similar to that observed for **2gt** (Figure 11A) and differs significantly from those observed for **2gg** and **2tg** (Figure 1). Thus, on the basis of considerations of conformational energy, **4** is not a good structural mimic of the **2gg** structure found commonly in nucleic acids. In **4**, *S* conformers appear slightly more stable than those of **2gt**. The shallow local energy minimum observed near  $^4E$  of **2gt** is more defined in **4** and appears shifted toward the  $E_3$  conformer. The global energy minimum conformers for **4** and **2gt** are identical ( $E_2$ ). Given the similar energy profile for **4** and **2gt**, structural comparisons are hereafter made between **4** and **2gt**.

Deoxygenation at O5 has no effect on the overall dependencies of C–H bond length on ring conformation, although some shifting of the curves is observed (see Supporting Information, Figure 5). Most notable is the shorter C3–H3 and the longer C4–H4 bonds in **4** than in **2gt** for essentially all ring forms, the latter presumably caused by the loss of a bond-length reducing 1,3-lone-pair effect involving O5 in **2gt**, similar to that depicted for **2tg** in Scheme 4 (C). Previous NMR studies of 5-*O*-methyl- $\beta$ -D-pentofuranoses and 5-deoxy- $\beta$ -D-pentofuranoses revealed a systematic change in  $^{13}C$  and  $^1H$  chemical shifts upon

(33) Cloran, F.; Carmichael, I.; Serianni, A. S., unpublished results.

(34) Carmichael, I.; Chipman, D. M.; Podlasek, C.; Serianni, A. S. *J. Am. Chem. Soc.* **1993**, *115*, 10863–10870.

(35) Church, T.; Carmichael, I.; Serianni, A. S. *Carbohydr. Res.* **1996**, *280*, 177–186.

(36) Bose, B.; Zhao, S.; Stenutz, R.; Cloran, F.; Bondo, P. B.; Bondo, G.; Hertz, B.; Carmichael, I.; Serianni, A. S. *J. Am. Chem. Soc.* **1998**, *120*, 11158–11173.

(37) Brameld, K. A.; Goddard, W. A., III. *J. Am. Chem. Soc.* **1999**, *121*, 985–993.

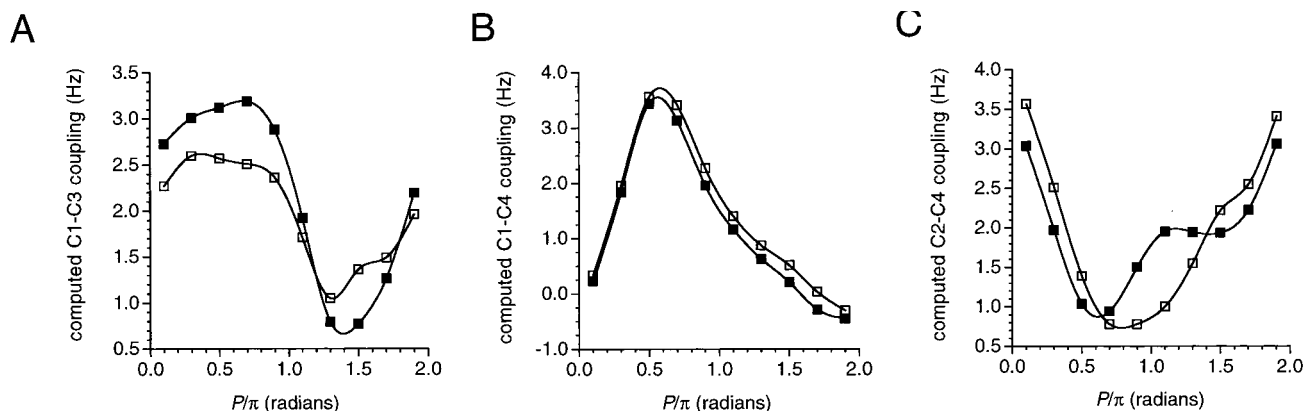


**Figure 10.** Computed  $^{2+3}J_{CC}$  values in **2gt** (solid squares) and **2gg** (open squares) determined from density functional theory (optimized geometries: B3LYP/6-31G\*;  $J$ -coupling calculations: B3LYP/[5s2p1d,2s]). (A)  $^{2+3}J_{C1,C3}$ . (B)  $^{2+3}J_{C1,C4}$ . (C)  $^{2+3}J_{C2,C4}$ .

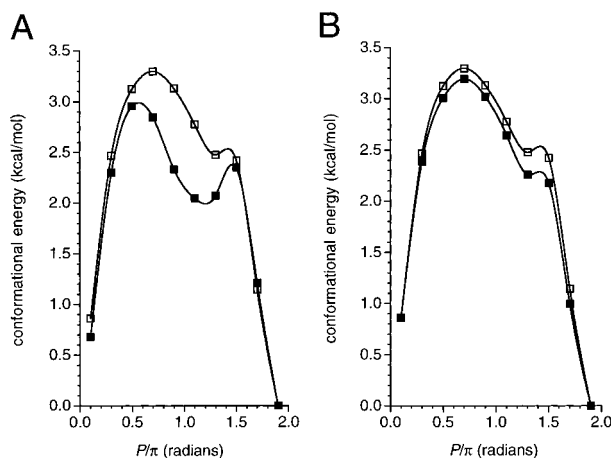


**Figure 11.** Conformational energy profiles for (A) **4** (closed squares) and **2gt** (open squares) (HF/6-31G\*) and (B) **5** (closed squares) and **2gt** (open squares) (HF/6-31G\*). One full rotation around the pseudorotational itinerary is equivalent to 0–2  $P/\pi$ , where 0.1  $P/\pi = ^\circ E$ , 0.3  $P/\pi = E_4$ , 0.5  $P/\pi = ^\circ E$ , and so forth (Scheme 1).

C5-deoxygenation.<sup>38</sup> An alternating shielding–deshielding–shielding pattern was observed for the C4–C3–H3 ring fragment, respectively, upon C5 deoxygenation, with larger than expected effects observed at the more remote C3–H3 fragment. The latter shielding is observed regardless of ring configuration, that is, in structures having H3 cis and trans to C5, suggesting a through-bond mechanism. These chemical shielding effects may be mediated partly by the above-noted changes in C–H bond length.

As observed for C–H bond lengths, the effect of ring conformation on endocyclic and exocyclic C–O bond lengths in **4** and **2gt** is identical, although some shifting of the curves is noted (see Supporting Information, Figure 5). The C1–O1 curves are virtually identical, but a small increase in the C3–O3 bond length is observed in **4**, which may be correlated to the above-noted shorter C3–H3 bond in **4**. The C1–O4 bond length in **4** shows a more significant local decrease in west forms near  $E_0/1E$  (relative to that in **2gt**), while the C4–O4 curve shows a uniform shift to slightly longer bonds in **4** relative to that in **2gt**.

The endocyclic C–C bond lengths in **4** and **2gt** show an identical dependence on ring conformation with respect to trends and absolute values, but the C4–C5 bond length in **4** is displaced uniformly to larger values (see Supporting Informa-

tion, Figure 6). Substitution of CH<sub>3</sub> for CH<sub>2</sub>OH in **2** causes a systematic decrease in the C1–O4 bond length (for most conformers), an increase in the C4–O4 bond length, and an increase in the C4–C5 bond length. It is interesting to note that  $^1J_{C5,C6}$  values in D-glucopyranoses are larger (43.0–43.6 Hz) than corresponding  $J$ -couplings in 6-deoxy-D-glucopyranoses (40.9–41.2 Hz).<sup>36</sup> While the extent of this difference will depend on the distribution of C5–C6 rotamers in the former due to the influence of the O–C–C–O torsion angle on  $^1J_{CC}$ ,<sup>34</sup> the smaller  $^1J_{CC}$  in the deoxy analogue appears consistent with the longer C–C bond found in these structures (this effect is commonly attributed qualitatively to the loss of an electronegative substituent on the C–C fragment,<sup>34,39</sup> but the underlying cause may reside in the resulting C–C bond elongation).

The C4–O1–C1 bond angle in **4** shows the same dependence on ring conformation as observed in **2gt**; absolute values are also identical. Puckering amplitude ( $\tau_m$ ) as a function of phase angle,  $P$ , for **4** and **2gt** is also virtually identical (see Supporting Information, Figure 7).

Overall, the energetic and structural properties of **4** and **2gt** are very similar, thereby demonstrating that **4** is a better mimic of **2gt** than of **2gg** or **2tg**. This result can be explained by noting that, in **2gt**, O5 is pointing “away” from the furanose ring, and thus its (through-space) effects on ring conformation and structure are expected to be small. Consequently, the loss of O5 would be expected to result in only small changes in conformational energy and structural parameters via through-bond mechanisms.

**2. Methyl Glycosidation.** It is well known that glycosidation of reducing sugars reinforces the anomeric effect in both aldofuranosyl and aldopyranosyl rings.<sup>23–25</sup> We reasoned that this effect might introduce additional stability to ring conformers of **2** having the C1–O1 bond quasi-axial or near quasi-axial, thus affecting the conformational energy profile, as suggested from prior experimental studies.<sup>25,40</sup> To examine this possibility, ab initio calculations were conducted on **5** (*gt* rotamer) and the resulting energy and structure parameters compared to those found previously for **2gt**.

Contrary to expectation, the conformational energy curves for **5** and **2gt** are virtually identical, with both showing a global energy minimum at  $E_2$  and a local energy minimum at  $^4E$  (Figure 11B). Energies of S forms of **5** are slightly lower than observed for the same forms of **2gt**. Methyl glycosidation, therefore, failed to introduce additional stability to forms containing a quasi-axial C1–O1 bond; at least in **2gt**, methyl

(38) Snyder, J. R.; Serianni, A. S. *Carbohydr. Res.* **1987**, 163, 169–188.

(39) Duker, J.; Serianni, A. S. *Carbohydr. Res.* **1993**, 249, 281–303.

(40) Serianni, A. S.; Barker, R. J. *Org. Chem.* **1984**, 49, 3292–3300.

glycosidation exerts virtually no effect on preferred conformation in these *in vacuo* calculations.

All endocyclic C–H bond lengths show the same dependence on ring conformation in **5** and **2gt**; absolute values are also virtually identical (see Supporting Information, Figure 8). Only the C1–H1 bond length changes noticeably upon glycosidation and is uniformly longer in **5**. It is interesting to note that, in the conversion of 5-*O*-methyl-D-pentofuranoses to methyl D-pentofuranosides,  $\delta_{\text{H1}}$  shifts upfield by  $\sim 0.35$  ppm, while all other  $^1\text{H}$  chemical shifts remain essentially unaltered upon glycosidation in configurations having O1 *cis* to C5.<sup>38</sup> The change in C1–H1 bond length upon conversion of **2gt** to **4gt** may be partly responsible for this  $\delta_{\text{H1}}$  effect.

Both C–O bonds involving C1 are affected by methyl glycosidation (see Supporting Information, Figure 8), but the overall dependencies on ring conformation are identical. The C1–O1 bond is uniformly shorter in the glycoside. The decrease in C1–O4 bond length in western conformers is more pronounced in **5** than in **2gt**. The C4–O4 bond length shows the same dependence on ring conformation in **5** and **2gt**, but a small decrease is observed uniformly in the glycoside; in contrast, the C3–O3 and C5–O5 curves are nearly superimposable for **5** and **2gt** (see Supporting Information, Figure 9).

In contrast to the comparatively large overall change in C1–O1 bond length in **5** with ring conformation, the O1–CH<sub>3</sub> bond exhibits only a very small change (See Supporting Information, Figure 8). Its dependence on ring conformation is biphasic, with minima located at  $^3\text{E}$  and  $\text{E}_3$ , and maxima located at  $^0\text{E}$  and  $\text{E}_0$ .

Puckering amplitude ( $\tau_{\text{m}}$ ) and the C4–O4–C1 bond angle remain essentially the same in **5** and **2gt**, as do the endo- and exocyclic C–C bond lengths (see Supporting Information, Figures 10 and 11). Very little change in C1–O1–CH<sub>3</sub> bond angles is observed in the different ring conformers of **5** (data not shown).

The C1–O1 torsion angle exhibits essentially the same dependence on ring conformation in **5** and **2gt** but is shifted to smaller values in **5** (see Supporting Information, Figure 12), presumably in response to the greater steric demand of the methyl aglycone. The remaining exocyclic torsions (C3–O3, C5–O5, C4–C5) are virtually identical in **5** and **2gt**.

Overall, methyl glycosidation exerts minimal effects on the conformational energy and structure of **2gt**, with most of the minor structural changes occurring in the vicinity of C1 (e.g., C1–H1 bond lengthened; C1–O1, C1–O4, and C4–O4 bonds shortened).

## Conclusions

This investigation has examined the effect of three structural variables on the conformational energies, structural parameters, and  $J_{\text{CH}}$  and  $J_{\text{CC}}$  NMR spin-couplings in 2-deoxy- $\beta$ -D-erythro-pentofuranose **2** using molecular orbital theory (HF/6-31G\* and B3LYP/6-31G\* for geometry optimization; B3LYP/[5s2p1d,2s] for  $J$ -coupling calculations): rotation about the C4–C5 bond (hydroxymethyl conformation), deoxygenation at C5, and methyl glycosidation. A number of useful observations evolved from this work, which are summarized as follows:

(a) Rotation of the C4–C5 bond exerts major effects on the conformational energy and structure of **2**. Overall conformational profiles differ significantly for **2gg**, **2gt**, and **2tg**. Importantly, **2gg** yields an energy profile consistent with a two-state exchange between N and S forms having comparable energies, that is, a conformational model consistent with the common assumption underlying the treatment of NMR  $J$ -couplings in furanose rings. In contrast, **2gt** and **2tg** yield energy

profiles in which only one geometry, or a group of similar geometries, is highly preferred. In solution, solvation may play a key role in affecting these profiles; in the present study only the *intrinsic* intramolecular forces within **2** have been probed, and only a few of the available degrees of freedom have been inspected. It is possible that, upon inspection of the complete energy surface or upon inclusion of solvation effects, **2gt** and **2tg** may display behavior more consistent with a two-state N/S model, but this issue remains to be addressed.

Prior NMR studies have led to estimations of the populations of hydroxymethyl group rotamers in methyl 2-deoxy- $\beta$ -D-erythro-pentofuranoside **5** and 5-*O*-methyl 2-deoxy- $\beta$ -D-erythro-pentofuranose **6** in aqueous solution.<sup>41,42</sup> In both **5** and **6**, the *gt* conformer appears to be most abundant ( $\sim 50\%$ ), with the *gg* and *tg* rotamers approximately equally populated at  $\sim 25\%$ . These experimental findings are at odds with the relative stabilities of **2gg**, **2gt**, and **2tg** predicted by the present calculations, where **2gg** is found to be marginally more stable than **2gt** and **2tg**. This discrepancy suggests a potential role of solvent in influencing these rotamer distributions or to limitations in the conventional experimental application of  $^3J_{\text{HH}}$  values used to estimate these populations.

The conformational preferences of aldopentofuranosyl rings, of which **2** is an example, will be influenced by several structural factors,<sup>40</sup> including stereoelectronic anomeric and gauche effects.<sup>23,24</sup> In **2**, the ring oxygen (O4) plays a central role in the latter effects, being involved *simultaneously* in two gauche effects with O3 and O5, and in an anomeric effect with O1. Ring conformation modulates the anomeric effect and gauche effect with O3, whereas C4–C5 bond rotation modulates the gauche effect with O5. Thus, a complex interplay of stereoelectronic forces is at work in **2**; the strength of each of these factors is likely to be influenced by the nature of the remaining two. For example, rotation of the C4–C5 bond in **2** may modulate the strength of the anomeric effect by influencing the electronic character of O4. A quantitative determination of the effect of overall molecular structure on each of these stereoelectronic factors will require systematic studies of deoxy analogues of **2** (i.e., removal of O3 or O1). It would be useful, however, to quantify these effects to establish the nature of the interplay between them and how this interplay ultimately directs geometric preference.

While not discussed in this report, the present HF/6-31G\* calculations suggest the possible presence of C–H hydrogen bonds in west conformations of **2tg** (between O1 and H5S) that may play a role in stabilizing these structures. The role of this type of hydrogen bonding in dictating carbohydrate conformation is presently unknown, but given the high concentration of electronegative substituents in saccharides, it is conceivable that some C–H bonds will be sufficiently polarized to promote these interactions under some conditions. This potential structural factor is worthy of further investigation.

(b) Rotation of the C4–C5 bond has allowed further exploration of the factors affecting C–H, C–C, and C–O bond lengths in furanoses. The influence of 1,3- and 1,4-oxygen lone pair effects on these bond lengths, which were identified in previous work,<sup>10,22</sup> has been confirmed. It should be appreciated that furanose rings are ideal test systems with which to evaluate structural factors affecting saccharide molecular geometry. The conformational flexibility of these rings allows straightforward and systematic sampling of a full range of bond orientations in

(41) Kline, P. C.; Serianni, A. S. *Magn. Reson. Chem.* **1990**, 28, 324–330.

(42) Serianni, A. S.; Kline, P. C.; Snyder, J. R. *J. Am. Chem. Soc.* **1990**, 112, 5886–5887.



structures along the pseudorotational itinerary that are energetically similar, in contrast to pyranose rings where such changes are made less easily and systematically and yield structures highly dissimilar in energy.

(c) The results of this and previous work serve to emphasize the significant effects that bond rotations exert on the energies and structures of saccharides. Meaningful comparisons between different structures can only be made when the states of all potentially rotatable bonds (with the exception of that which has been purposely altered to evaluate its effect) are similar between the compared structures. Unintended torsional changes can occur spontaneously in geometric optimizations of saccharides and appear to be driven largely by the formation of intramolecular hydrogen bonds. Failure to identify, and correct or account for, these changes can lead to inappropriate and misleading structural arguments or conclusions.

(d) The comparison of NMR  $J$ -couplings involving  $^{13}\text{C}$  ( $J_{\text{CH}}$  and  $J_{\text{CC}}$ ) in **2gt** and **2gg** provides new and valuable information on the effect of C4–C5 bond rotation on scalar couplings in **2**. This comparison is essential to ongoing efforts to interpret these parameters in nucleic acids for which additional experimental conformational constraints would be beneficial. Of all  $J$  couplings examined,  $^1J_{\text{CH}}$  appear most affected by this rotation, presumably because substantial changes in C–H bond length accompany the rotation, in large part mediated by oxygen lone-pair effects. These bond length changes appear to exert less influence on  $^2J$  and  $^3J$  values. Importantly, overall correlations between  $J$  magnitude and ring conformation are conserved for all couplings examined, and deviations, when observed, are predictable on the basis of the findings of prior work. Predictions of the effect of C4–C5 bond rotation on  $J$ -couplings within the ring and hydroxymethyl group<sup>9a,b</sup> have been fulfilled in this study, lending credibility to the rules for calculating/predicting these couplings in new structures, and providing renewed incentive to further develop these parameters as NMR probes in nucleic acids. One factor that remains to be examined is the effect of  $O$ -phosphorylation on these couplings, and efforts are underway to examine this factor experimentally and theoret-

cally. The latter effort will help fulfill the long-term goal of developing an integrated, computerized analysis of the multiple  $J$ -couplings within these rings to improve the assignment of preferred geometry and motional properties in solution.

(e) The conformational energy profile and structural parameters observed in the dideoxy analogue **4** closely resemble those observed in **2gt**, but differ significantly from those observed in **2gg** and **2tg**. These observations lead to the conclusion that the use of **4** as a simple structural mimic of the 2-deoxyribofuranose ring in DNA in experimental and theoretical investigations is not justified, since C4–C5 bond conformation is *gg* in the biopolymer.

(f) Methyl glycosidation of **2** does not cause significant changes in conformational energy profile and structural parameters. An enhanced anomeric effect, as manifested in a selective, increased stabilization of conformers containing a quasi-axial C1–O1 bond, is not observed, at least not for **2** in these gas-phase calculations. As noted above, solvation effects may induce such an effect in solution, as suggested by NMR results,<sup>25,40</sup> but the *intrinsic* forces in **2** do not appear to dictate such a change upon methyl glycosidation. It is possible that, in other ring configurations and substitution patterns, these effects will manifest themselves in gas-phase calculations, since a complex interplay of comparatively weak forces dictates ring geometry in these compounds.

**Acknowledgment.** This work was supported by a grant from Omicron Biochemicals, Inc. of South Bend, IN, and by the Office of Basic Energy Sciences of the United States Department of Energy. This is Document No. NDRL-4245 from the Notre Dame Radiation Laboratory.

**Supporting Information Available:** Figures (12) showing selected bond lengths, angles, and torsions as a function of ring conformation in **2**, **4**, and **5** (PDF). This material is available free of charge via the Internet at <http://pubs.acs.org>.

JA002525X